Magnetic Hybrid Carbon via Graphitization of Polystyrene-co-Divinylbenzene: Morphology, Structure and Adsorption Properties

UNIVERSITÀ DEGLI STUDI DI TORINO

ChemistrySelect,

Volume 1, Issue 10

July 1, 2016

Pages 2536–2541

DOI: 10.1002/slct.201600278

ChemistrySelect (Wiley),
Volume 1, Issue 10, July 1, 2016, Pages 2536–2541;
DOI: 10.1002/slct.201600278

Magnetic Hybrid Carbon via Graphitization of Polystyrene–co-Divinylbenzene: Morphology, Structure and Adsorption Properties

Federico Cesano,* Mastabur M. Rahman, Fabrizio Bardelli, Alessandro Damin, and Domenica Scarano[a]

Multilayer graphitic nanosheets/nanoshells have been obtained via pyrolysis at 850 8C of poly(4-ethylstyrene-co-divinylbenzene) (PS-co-DVB) by inflowing Fe(II)-acetylacetonate ($Fe(ACAC)_2$) into the pores of the polymer. Iron-free PS-co-DVB was also pyrolyzed at the same temperature, thus highlighting the effective role of the catalyst in promoting the graphitization at relatively moderate temperatures. It will be shown that under longer annealing times at 850 8C in presence of Fe_3C and a-Fe the carbon precursor undergoes an extensive graphitization as compared to the iron-free material. Catalyst nanoparticles were found to be encapsulated into graphitic nanoshells providing effective barriers to the oxidation processes, thus preserving the magnetic properties. On the other hands, the metallic nanoparticles can be oxidized under environmental conditions, with negative effects on the magnetic properties, which points out the need to preserve the material for applications. The hybrid multilayer graphitic carbon, tested in magnetically driven adsorption experiments of methylene blue dye, can find application in the water purification processes.

1. Introduction

Hybrid nanostructures have received an increasing interest due to their improved properties, which are explained with the synergistic effect due to the coexistence of different nanomaterials and then nanostructures.[1] In this regard, a very wide range of new applications is possible, including electrical, optical, magnetic devices and imaging probes.[2] As for the many constituents of the hybrid nanomaterials, carbon materials have attracted considerable attention because of the variety of structures, moving from 0D to 3D (fullerenes, carbon dots, nanoonions, nanocapsules, carbon nanotubes, graphenes, diamond, graphite, hybrid systems, etc.).[3] Due to the fact that each carbon structure may exhibit peculiar characteristics, the advantages to be gained include electrical and thermal conductivity, chemical inertness, low-weight, mechanical resistance catalytic processes, sorption characteristics, etc.[4] As far as environmental issues are concerned, dyes are known to be used in textile plants for more than 10,000 tonnes/year and approximately 100 tonnes/year of dyes are discharged into the water.[5] Nowadays, the removal of organic pollutants from water by means of the pollutant uptake is a topic at the forefront of the environmental research,[6] and looking into the future, dye sorbents will be even better effective and cleaner processes will be adopted. Even so, many textile industries actually use activated carbons for the treatment of waste by the adsorption of dyes from wastewater[7] and pyrolitic carbons from biomass derivatives (i.e cellulose, glucose, cyclodextrins) and polymer precursors[8] are a matter of a broad and significant interest, particularly for the design and synthesis of multi-functionalized carbons. Along these materials porous carbons, graphitic carbons obtained via catalytic graphitization may possess many advantages, including high surface area, thermal stability and can be produced by moderate energy-comsumption under relatively low temperature (as low as 800–1000 8C).[9] However, the interest on these graphitic materials has not been focused so far on advantages provided by magnetically guided systems.

Taking into consideration this aspect and considering traditional materials for water remediation, the present study is focused on the production at relatively moderate temperature (~ 850 8C) of multilayer graphitic nanoshells, with hybrid structure, peculiar porosity and magnetic properties, by starting from an abundant polymer. Furthermore, the uniform dispersion of the graphitization catalyst is favoured by the specific crosslinked and porous nature of the poly(4-ethylstyrene-co-divinylbenzene) (PS-co-DVB) allowing the incoming molecules to enter. Furthermore, the graphitization catalyst gives rise to magnetic nanoparticles. More interestingly, the hybrid character of the multilayer graphitic carbon, together with the mesoporous properties and the magnetic nature, can make it suitable for magnetically driven processes, including water purification from methylene blue dye.

[a] Dr. F. Cesano, Dr. M. M. Rahman, Dr. F. Bardelli, Dr. A. Damin,

Prof. D. Scarano
Dept. of Chemistry, NIS (Nanostructured Interfaces and Surfaces) Interdepartmental Centre,
University of Torino
Via P. Giuria, 7, 10125 Torino, Italy
E-mail: federico.cesano@unito.it

2. Results and Discussion

Thermal evolution of the PS-co-DVB and of Fe (II)/PS-co-DVB systems via TGA measurements.

Thermogravimetric profiles of PS-co-DVB and of Fe (II)/PS-co-DVB are reported in Figure 1. Carbon yields of about 10 wt% have been obtained for both samples at 850 8C before the isothermal steps. After the second isotherm (iii-step, in air flow) no residue remains from the pure sample, while the thermally treated Fe(II)/polymer exhibits a residual weight of about 1.4 %wt (i. e. iron oxide). From this, the amount of metal iron has been calculated to be about 1 %wt in the native sample. In addition, by comparing the two TGA profiles during the heating up to 850 8C, there is no evidence of significant differences. On the contrary, the weight percentage curve decreases linearly upon isothermal heating under N_2 for the Fe(II)/PS-co-DVB sample, while the same does not change over time for the pure polymer. It will be shown that the weight decrement, calculated to be ~3 % after 5 h, is plausibly associated with catalytic processes occurring at high temperature.

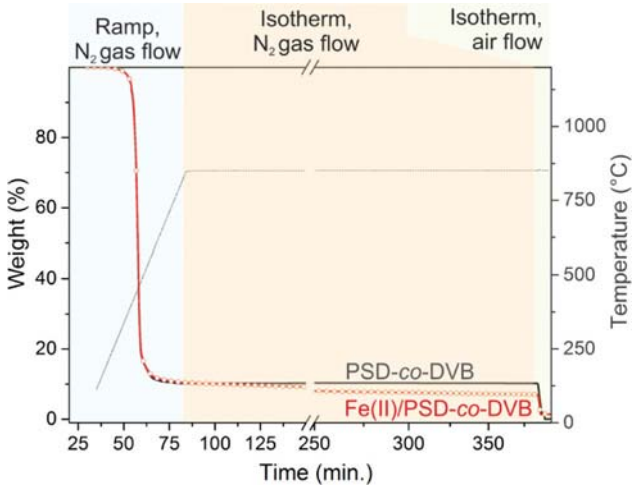

Figure 1. TGA profiles of PS-co-DVB (dark grey line) and of Fe(II)/PS-co-DVB (red line) during the treatment steps: (i) heating up to 850 8C under N_2, (ii) isotherm under N_2 flow for 5 h and (iii) isotherm for 0.5 h in air. The temperature profile of the experiments is also reported (light gray dotted line).

Due to the fact that the organic matter undergoes to complete pyrolysis under inert conditions upon quite mild treatments (~400-800 8C),[10] and that the pyrolysis is accompanied by the elimination of volatile species (i. e. even containing H, O, N), the conversion of polymers into carbon materials largely depends on the nature of the carbon precursor and of the catalyst. In this regard, the mobility of the polyaromatic basic structural units (BSUs) under formation is accompanied by the formation of small or more extended p-electron systems.[11] In this domain, the structural properties of pyrolized materials have been investigated.

Structure of the annealed PS-co-DVB and of Fe(II)/PS-co-DVB systems via Raman and XRD analyses.

Raman spectra of PS-co-DVB and Fe(II)/PS-co-DVB samples treated at 850 8C for 0.5 h, 2 h and 5 h are reported in Figure 2a and b, respectively.

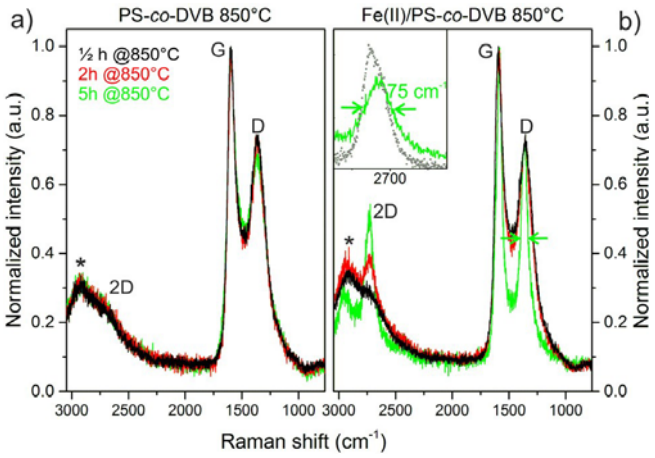

Figure 2. Raman spectra of: a) PS-co-DVB and b) Fe(II)/PS-co-DVB treated at 850 8C for 0.5 h (black line), 2 h (red line) and 5 h (green line). The intensities of the Raman spectra have been normalized to the G-band. In the inset of b) the Raman spectrum of graphite (grey line) is compared with the 2D band region.

The carbonized PS-co-DVB shows the distinctive fingerprints of the carbon materials, due to the G-band and D–band, occurring at ~1595 cm^{-1} and at ~1360 cm^{-1}, respectively, and an additional broad envelope (2D-band) at higher energy (2600-2800 cm^{-1}) (Figure 2a). The envelope, during the isothermal heating, sharpens into two distinctive features at ca. 2720 cm^{-1} (more intense) and at 2975 cm^{-1} for the thermally treated Fe (II)/PS-co-DVB (Figure 2b).

The G-band, usually falling at 1580 cm^{-1} in the hexagonal graphite, is attributed to the in-the-plane stretching vibrations of sp^2-bonded carbon atoms (E_{2g} mode). The D-band, located at lower energy, is a disorder-induced feature and its intensity depends on the presence of topological and structural defects.[11a] The I_D/I_G ratio (D/G area ratio for the more crystalline samples) and the full-width-at-half-maximum (FWHM) of bands is an useful indicator of the overall crystallinity.[12] In particular the decreasing of both I_D/I_G ratio and of the FWHM is explained with the smaller defectiveness and the larger sizes of graphitic crystallites or their sub-units.[13]

The appearance of the 2D band at about 2720 cm^{-1}, which is increasing with the annealing time for the Fe(II)/PS-co-DVB (Figure 2b), is also indicative of crystalline structures compatible with a multilayer graphitic nanosheet arrangement (with n > 2), whose properties are similar to those of graphene.[3] This fingerprint, usually not observed in more amorphous carbons,[3, 14] testifies the high crystallinity of the carbon material obtained from Fe(II)/PS-co-DVB. Notice that D- and G-bands of Fe(II)/PS-co-DVB treated at 850 8C sharpen with the annealing time (es-

pecially the D-band evidenced by arrows in Figure 2b), unlikely the carbonization process of the pure polymer. This is a clear indication of an increasing crystallinity and of more extended crystalline domains with the annealing time for the pyrolized Fe(II)/polymer. Furthermore, from a more accurate investigation of the 2D-band region a few considerations can be drawn for the Fe(II)-loaded polymer thermally treated at 850 8C for 5 h (inset of Figure 2b). It is known that the doublet structure (asymmetry) of the 2D peak of graphite is originated by the AB stacking order of the graphene planes, on the contrary the symmetry of the 2D band observed for the pyrolized Fe(II)/polymer, usually found in turbostratic graphite, is indicative of the absence of the AB stacking order.[15] In addition, from the FWHM value of this band, an average number of graphitic planes of more than 5 is expected.[15–16] Finally, the peak position of this band (at ◆2730 cm^{-1}) is compatible with the folded/curved nature of the graphitic stacks.[16]

From the Raman spectra of the PS-co-DVB sample (Figure 2a), no decrements of the FWHM are observed as a function of the annealing time, thus claiming the role of iron species in promoting the formation of crystalline carbon nanostructures. As Raman spectra are not informative on these species, XRD analysis has been performed.

XRD patterns of the pure polymer and of the Fe(II)/PS-co-DVB carbonized at 850 8C for 0.5 h and 5 h are reported in Figure 3.

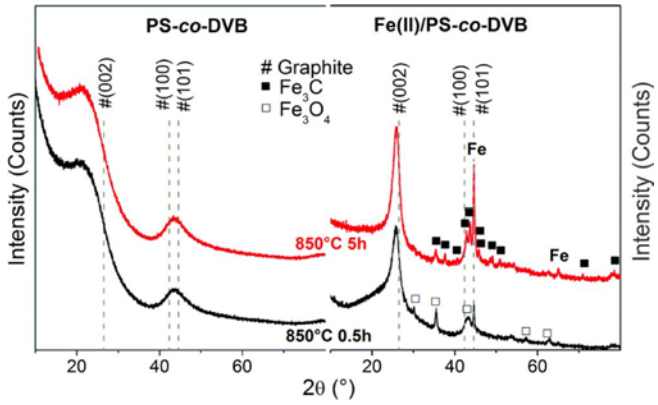

Figure 3. XRD patterns of: the polymer (left side) and Fe (II)/PS-co-DVB (right side) treated at 850 8C for 0.5 h and 5 h. Peak positions of the reference materials: magnetite (& Fe_3O_4, PDF n. #019-0629), iron carbide (& Fe_3C, PDF n. #35-0772), metal iron (bcc-phased Fe, PDF n. #06-0696) and hexagonal graphite (vertical dotted lines), are reported for comparison.

XRD patterns of the carbonized polymer at 850 8C (left side on Figure 3), exhibit two very broad features. The first one, ranging in the 10 ::: 2q ::: 30 interval, is assigned to the (002) plane reflections of sp^2-C in the graphitic arrangement, whereas the wide peak, in the 40 ::: 2q ::: 50 range with a maximum at about 2q ffi 44, can be assigned to the convolution of the (100)/(101) XRD diffraction planes of graphite, which sometimes is called (10) band.[11a, 17] The wide character of these two features is typically observed in amorphous carbon phases or non-graphitizable carbon materials.[17b, 18] XRD patterns of the Fe (II)/PS-co-DVB treated at 850 8C for 0.5 h and 5 h are shown on the right side of Figure 3. Besides the narrower XRD reflections observed at lower angles, some additional peaks, with maxima at 2q ffi 30, 35.2, 42.9, 56.9 and 62.5 appearing after 0.5 h of thermal treatment, are assigned to (220), (311), (400), (511), and (440) planes of magnetite-Fe_3O_4 (PDF n. #019-0629). After a longer treatment, other narrow features at 2qffi 35.3, 37.6, 39.6, 40.5, 43.6, 45.7, and at 2qffi44.6, 65, which are assigned to cementite (Fe_3C, PDF n. #35-0772) and ferrite (bcc-phased Fe, PDF n. #06-0696), are observed. The presence of these two iron-based species occurs with the higher crystallinity of the carbon phase, as testified by the sharp band in the 2q = 23–28 interval.

It is known that the XRD peak broadening depends on the size of the coherent scattering domains, therefore by applying the Sherrer's equation to the XRD reflection in the 10 ::: 2q ::: 30 interval, which is closer to the (002) diffraction peak of graphite, average crystallite sizes of domains along the c-axis direction were estimated for both the carbon samples (treated at 850 8C for 5 h), (from red patterns in Figure 3). Average values of about 1.1 nm (Fe-free sample) and 4.6 nm (Fe-rich sample), were obtained. In addition, by considering an interlayer distance of 0.335 nm, an average stacking number of layers can be estimated to be n ffi 3 and n ffi 13 for the carbonized polymer and Fe(II)/PS-co-DVB, respectively. Due to the peak overlapping in the 2q ffi 40-76 range, the crystallite sizes along the xy-plane direction cannot be determined.

From these observations, it can be inferred that the pyrolysis of Fe(II)/PS-co-DVB gives nanoparticles of Fe_3O_4 and a turbostratic amorphous carbon. Then, the reduction of Fe_3O_4 to Fe_3C and ferrite (a-Fe) with the simultaneous catalysed graphitization of the carbonaceous phase is occurring with the annealing time. The catalyst evolution during the annealing temperature, which is higher than Fe-C and Fe – Fe_3C eutectoid temperatures (740 8C and 727 8C, respectively), can be rationalized as influenced by kinetic effects and discussed in the context of the bulk Fe – C phase, as reported by recent results.[19] Some more the presence of metastable iron carbide (Fe_3C) on the XRD pattern suggests that carbides are highly active in the catalytic graphitization process of biomass and polymers, as reported for various transition metal catalysts (e. g. Fe, Ni, Co, etc.) treated in the 500–900 8C temperature interval.[4a, f, 8a, 10b, 20] While these metals are active in forming metastable carbides, the formation of crystalline carbons (CNTs, graphene) has also been reported in presence of Au, Ag, Pd, Pt via a phase segregation mechanism.[21]

In order to highlight the role of the graphitization catalyst and the effect of the pyrolysis temperature, pyrolized samples of the crosslinked polymer and of Fe(II)/PS-co-DVB have also been obtained at different temperatures. From the XRD pattens of sample treated at 600 8C, 850 8C, 1100 8C and at 1500 8C (Figure S1, Supporting Information), it is clear that the graphitization process of the pyrolized material starts at lower temperature as compared to the iron-free polymer, which retains a short-range ordered structure. Due to the presence of iron carbide and metal phases in the XRD patterns, however, the high

graphitization degree (i. e. large stacked hexagonal carbon layers with a three-dimensional regularity) cannot be ruled out.

Morphology of the annealed PS-co-DVB and Fe(II)/PS-co-DVB samples via SEM and TEM measurements.

SEM images of the carbon-based materials obtained from the thermal treatments at 850 8C for 5 h are shown in Figure 4a,b.

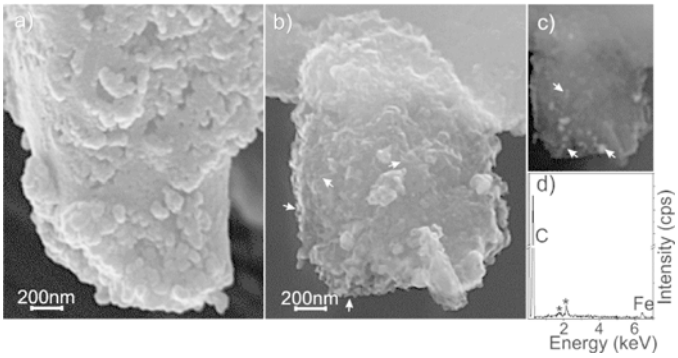

Figure 4. SEM images of carbon materials obtained from: a) PS-co-DVB and b) Fe(II)/PS-co-DVB treated at 850 8C for 5 h; c) backscattered electron image of the region shown in b); d) EDAX spectrum of the region shown in b). Arrows in both b) and c) images illustrate irregular/thin nanostructures and regions associated with Fe-rich nanoparticles. Asterisks in the EDAX spectrum are related to Au coming from the metal sputtering for SEM imaging.

The thermally treated PS-co-DVB shows an irregular surface constituted by aggregates of apparently rounded nanostructures 30–50 nm in size (Figure 4a), which are much more rare for the annealed Fe(II)/PS-co-DVB (Figure 4b). The sample, in fact, is dominated by thin nanostructures evidenced by arrows in Figure 4b. The same area imaged by secondary electrons in Figure 4b, has also been acquired by backscattered electrons (Figure 4c). In this image, the contribution of heavy-element (bright regions) is evidenced by arrows, which has been assigned to iron species, according the EDAX spectrum acquired on this selected area (Figure 4d). The amount of Fe is roughly estimated to be around 1 %wt, in agreement with TGA analysis.

To gain more information at the atomic scale, the Fe (II)/PS-co-DVB annealed at 850 8C for 5 h has been TEM and HRTEM imaged, as shown in Figure 5. An irregular morphology made by curved structures and by nanoparticles with sizes ranging in the 10 -7 40 nm interval can be observed in the lower resolution TEM image (Figure 5a). Graphitic multilayers form a porous scaffold with crystalline nanoshells, as shown from the lattice fringes 3.4 A spaced, corresponding to the (002) planes of the graphitic carbon (Figure 5b,c). A core/shell structure made by a well shaped nanoparticle, which is encapsulated in curved crystalline graphitic layers, is shown (Figure 5c). The nanoparticle is fast-Fourier-transform (FFT) imaged in Figure 5d. The diffraction spots on the selected area in c) are shown according to a regular symmetry. From the corresponding simulated electron diffraction patterns (Figure 5e), reflections corresponding to the

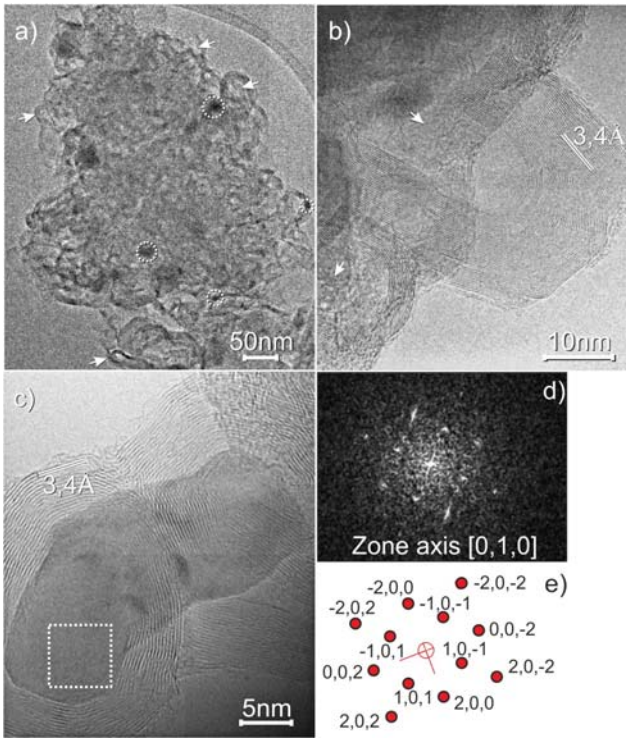

Figure 5. a) Low-resolution TEM image of the Fe(II)/PS-co-DVB treated at 850 8C for 5 h; arrows and white dashed circles show porous cavities and nanoparticles, respectively; b) HRTEM image of curved graphitic nanoshells; arrows evidence enclosed cavities; c) HRTEM image of a well shaped nanoparticle encapsulated in the hybrid graphitic carbon nanoshells; d) FFT image of the selected area in c); e) the corresponding simulated electron diffraction pattern of the orthorhombic iron carbide (Fe3C, cementite) along the [0,1,0] zone axis direction.

{101} and {202} planes families along the [010] zone axis, confirm that the selected nanoparticle is compatible with the orthorhombic iron carbide (Fe_3C).

The presence of Iron-based nanoparticles in isolated graphitic nanoshells confirms their ability to take up carbon atoms from the amorphous carbon phase to form metastable Fe_3C, as reported in some papers.[4a,8a,c,19] Then, carbon atoms may undergo a complete segregation as graphitic nanoshells, due to the higher thermodynamic stability of the graphitic phase with respect to Fe_3C.

The peculiar porosity, the graphitic scaffold of the Fe(II)/PS-co-DVB treated at 850 8C for 5 h and its hybrid structure, suggest the investigation of additional properties, such as porosity and magnetic properties.

Surface area, porosity of the annealed polymer and of the hybrid graphitic material treated at 850 8C.

Volumetric N_2-adsorption/desorption isotherms of the PS-co-DVB and of Fe(II)/PS-co-DVB treated at 850 8C for 5 h are shown in Figure S2 (Supporting Information) and surface area/porosity properties of the samples are reported in Table 1.

From the isotherms, it is clear that the two samples have different porosity properties. In fact, from the shapes of the ad-

Table 1. BET surface area and porosity properties of the thermally treated samples.

	S_{BET} [a] (m^2/g	S_{micro} [b] (m^2/g)	S_{meso} [b] (m^2/g)	% $_{Smeso}$ [c]	V_{Tot} [d] (cm^3/g)
PS-co-DVB @850 8C, 5 h	354	350	4	1	0.1707
Fe (II)/PS-co-DVB @850 8C, 5 h	303	149	154	51	0.2313

[a] Evaluated in the 0.1 < P/P0 < 0.3 pressure range; [b] Estimated using the t-plot method (carbon black STSA thickness curve); [c] $\%(_{Smeso}) = S_{meso}/S_{BET}$ x100; [d] Total pore volume (VTot) calculated as the volume of the liquid at P/P0 » 0.975

sorption/desorption branches and hysteresis loops, the carbonized polymer is basically microporous (Figure S2a Supporting Information), while a mixed microporous/mesoporous character is inferred for the hybrid graphitic carbon (Figure S2b Supporting Information). Although a small reduction of the surface area (S_{BET}) is observed for the hybrid graphitic scaffold, its mesoporous character is prevailing as compared to the carbonized polymer. Pore size distributions (PSDs) of both samples, as obtained by the DFT model, are reported in Figure S2c (Supporting Information). From these distributions it is concluded that the carbonized polymer is basically dominated by a micropore contribution in the 10–14 A range, while the hybrid graphitic scaffold has a more complex pore size distribution. As a matter of fact, besides the micropore family in the 10–14 A range, a second distribution of micropores with sizes in the 10–20 A interval appears together with a wider and complex contribution of mesopores in the 20–100 A interval. These results were also confirmed by PSDs obtained by the Barrett-Joyner-Halenda (BJH) analysis (data not shown for the sake of brevity) and are in close agreement with the TEM results. Furthermore, the moderately high surface area and the mesopore volume are obtained for the catalyzed graphitic carbon, as compared with the parental porous systems.[9]

A specific area (S) of about 205 m^2/g has been calculated from the MB adsorption isotherm at RT for the hybrid sample (Figure S3, Supporting Information). The relatively lower value of S with respect to the S_{BET}, coming from the N_2 adsorption experiments, testifies that the dye adsorption isotherm can be considered only as an approximation of the surface area for this kind of materials exposing extensive aromatic domains, as discussed by other authors.[22] In fact, the inconsistency of the results, between dye and gas sorption procedures, can be explained with many effects, including specific dye-substrate interactions,[22b] between MB and aromatic regions of the graphenic domains.[23]

Magnetically guided methylene blue adsorption experiments of the hybrid graphitic carbon.

The mesoporous character of the hybrid graphitic carbon material looks ideal to test the adsorption of methylene blue that is an organic dyestuff commonly used for tracer studies in water purification research. In addition, the hybrid graphitic material shows macroscopic magnetic properties (Figure S4, Supporting Information). Magnetically guided systems, which can be moved by magnetic fields to achieve a desired spatial location, are materials suitable for many applications, such as wastewater purification, catalysis, photocatalysis, magnetic resonance imaging, release of active species/drug delivery processes.[4a, e, 24] Magnetic properties of the hybrid graphitic carbons are associated with iron and cementite nanoparticles,[4b, e, 8b, 25] which have been found to be encapsulated in graphitic shells, thus preserving the nature of the magnetic nanoparticles.

A methylene blue water solution (25 mg/l, 100 ml) was examined in the UV-vis range for selected contact times with 24 mg of the hybrid graphitic carbon (Figure 6). From this figure, the intensity of the two main MB bands (at ~608 nm, ~660 nm) that are assigned to monomeric/aggregated species,[2c] is decreasing with the MB contact time. Althought a detailed assignment of these bands is outside the scope of this work, it is noteworthy that a new band appears with the disappearance of MB fingerprints. Such feature, with maxima at ~265 nm is assigned to p-p* transitions of the C=C aromatic rings of C-sp^2.[3] This band has also been found for the same hybrid graphitic carbon obtained at 850 8C, dispersed in pure water (0.5 mg/ml) and monitored along the time (Figure S5, Supporting Information).

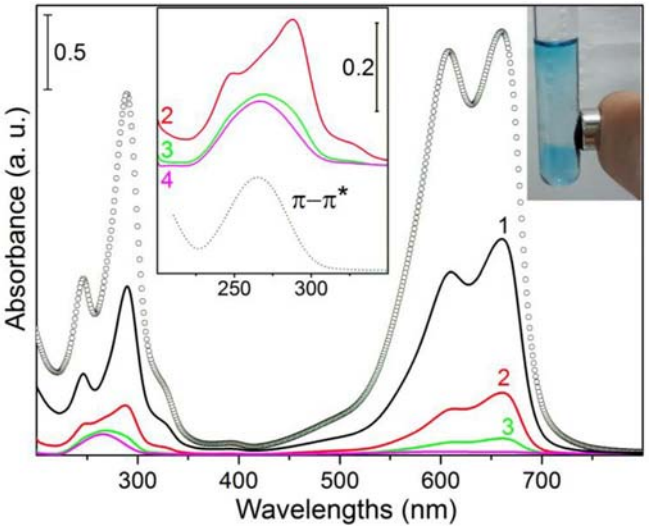

Figure 6. UV-visible spectra evolution of MB water solutions after being contacted with the hybrid multilayer carbon (24.3 mg) for selected time (1: 4 min, 2: 12 min, 3: 21 min, 4: 29 min); In the insets: a picture representing the magnetically guided experiment (top right panel) and an exploded view in the 200–400 nm interval (top centre panel). In this inset, the UV-vis spectrum of hybrid carbon obtained at 850 8C dispersed in pure water (0.5 mg/ml) is reported for comparison (grey dotted line).

3. Conclusions

In this work, a hybrid structure, made by encapsulating Iron-based nanoparticles in graphitic nanoshells, is obtained by a simple method. Hybrid multilayer graphitic carbons have been

obtained via pyrolysis at 850 8C of Poly(4-ethylstyrene-co-divinylbenzene) copolymer by inflowing Fe (II)-acetylacetonate into the pores of the polymer. Pyrolysis of Fe(II)/PS-co-DVB gives at first nanoparticles of Fe_3O_4 on amorphous carbon. Then, the reduction of Fe_3O_4 to Fe_3C and ferrite (a-Fe) with the simultaneous catalyzed graphitization of the carbonaceous phase is obtained by the annealing time. In fact, Fe nanoparticles are able to take up carbon atoms from the amorphous carbon phase to form metastable Fe_3C. During the process, carbon atoms undergo a complete segregation as graphitic nanoshells, due to the higher thermodynamic stability of the graphitic carbon with respect to Fe_3C. Finally, the porous scaffold made by Fe-based nanoparticles encapsulated in graphitic carbon nanoparticles with a core/shell structure, is able to provide effective oxidation barriers and to preserve the magnetic properties. The hybrid character of the multilayer graphitic carbon, together with the mesoporous properties and the magnetic nature can make it suitable for the controllable processing of water purification. In fact, the magnetically driven hybrid material has been shown to be effective in the removal of methylene blue in water solution.

Supporting Information Paragraph

Experimental Section and additional information (XRD patterns of the polymer treated at different temperatures without and with the graphitization catalyst, N_2-adsorption/desorption isotherms and pore-size distributions; Methylene blue adsorption experiments; Surface area determination of the hybrid carbon material from the MB adsorption experiments; Macroscopic magnetic properties of the hybrid porous graphitic powder; and UV-Vis spectra for the same hybrid graphitic carbon obtained at 8508C and dispersed in pure water suspension) are given in the Supporting Information.

Acknowledgements

This work was supported by MIUR (Ministero dell'Istruzione, dell'Università e della Ricerca), INSTM Consorzio and NIS (Nanostructured Interfaces and Surfaces) Inter-Departmental Centre of University of Torino. The authors thank Dr. Agostini G. and Mrs. Franconieri F. for their support in the TEM measurements.

References

[1] a) S. Cravanzola, G. Haznedar, et al., Carbon 2013, 62, 270–277; b) F. Cesano, D. Pellerej, et al., J. Photochem. Photobiol. A-Chem. 2012, 242, 51–58; c) F. Cesano, S. Bertarione, et al., Adv. Mater. 2008, 20, 3342–3348; d) G. Haznedar, S. Cravanzola, et al., Materials Chemistry and Physics 2013, 143, 47–52.

[2] a) F. Garello, F. Arena, et al., RSC advances 2015, 5, 34078–34087; b) M. J. Uddin, D. E. Daramola, et al., PSS-RRL 2014, 8, 898–903; c) S. Cravanzola, L. Muscuso, et al., Langmuir 2015, 31, 5469–5478.

[3] V. Georgakilas, J. A. Perman, et al., Chemical Reviews 2015, 115, 4744 – 4822.

[4] a) J. Liu, N. P. Wickramaratne, et al., Nature Mater. 2015, 14, 763–774; b) R. P. Chaudhary, S. K. Mohanty, et al., Carbon 2014, 79, 67–73; c) L. Settineri, F. Bucciotti, et al., Cirp Annals-Manufacturing Technology 2007, 56, 573–576; d) M. M. Rahman, F. Cesano, et al., Catalysis Today 2010, 150, 84–90; e) M. Reza Sanaee, E. Bertran, J. Nanomat. 2015, 450183; f) J.-S. Lee, S.-I. Kim, et al., ACS Nano 2013, 7, 6047–6055.

[5] M. T. Yagub, T. K. Sen, et al., WaterAir Soil Poll. 2012, 223, 5267–5282.

[6] A. Alsbaiee, B. J. Smith, et al., Nature 2016, 529, 190–194.

[7] M. T. Yagub, T. K. Sen, et al., Adv. Coll. Interf. Sci. 2014, 209, 172–184.

[8] a) J. Hoekstra, A. M. Beale, et al., Chem. Mater. 2015, 119, 10653–10661; b) U. Male, P. Srinivasan, Journal of Applied Polymer Science 2015, 132, 42540; c) E. Thompson, A. E. Danks, et al., Green Chem. 2015, 17, 551–556.

[9] a) M. Xie, J. Yang, et al., Carbon 2014, 7, 215–225; b) L. S. Zhang, W. Li, et al., J. Phys. Chem. C 2009, 113, 20594–20598; c) J. W. Long, M. Laskoski, et al., J. Mater. Chem. 2011, 21, 3477–3484; d) X. Xia, D. Chao, et al., Nano Letters 2014, 14, 1651–1658.

[10] a) C. Zhuo, Y. A. Levendis, Journal of Applied Polymer Science 2014, 131, 39931; b) N. I. Maksimova, O. P. Krivoruchko, et al., J. Mol. Catal. A-Chem. 2000, 158, 301–307.

[11] a) M. B. Vazquez-Santos, E. Geissler, et al., Carbon 2012, 50, 2929–2940; b) S. Bertarione, F. Bonino, et al., J. Phys. Chem. B 2009, 113, 10571–10574; c) K. Takai, M. Oga, et al., Physical Review B 2003, 67, 214202–214211.

[12] a) L. G. Cancado, A. Jorio, et al., Nano Letters 2011, 11, 3190–3196; b) G. Cravotto, D. Garella, et al., New Journal of Chemistry 2011, 35, 915–919.

[13] a) C. Jager, H. Mutschke, et al., Applied Physics a-Materials Science & Processing 2006, 85, 53–62; b) A. Cuesta, P. Dhamelincourt, et al., J. Mater. Chem. 1998, 8, 2875–2879.

[14] a) L. G. Cancado, K. Takai, et al., Carbon 2008, 46, 272–275; b) O. A. Voronov, K. W. Street, Diam. Relat. Mater. 2010, 19, 31–39.

[15] A. C. Ferrari, Sol. State Commun. 2007, 143, 47–57.

[16] Y. Hao, Y. Wang, et al., Small 2010, 6, 195–200.

[17] a) D. Zhai, H. Du, et al., Carbon 2011, 49, 725–729; b) Z. Q. Li, C. J. Lu, et al., Carbon 2007, 45, 1686–1695

[18] F. Cesano, M. M. Rahman, et al., Carbon 2012, 50, 2047–2051.

[19] C. T. Wirth, B. C. Bayer, et al., Chem. Mater. 2012, 24, 4633–4640.

[20] a) Y. V. Fedoseeva, L. G. Bulusheva, et al., Materials Chemistry and Physics 2012, 135, 235–240; b) N. Amini, K. F. Aguey-Zinsou, et al., Carbon 2011, 49, 3857–3864; c) I. Stamatin, A. Morozan, et al., Physica E-Low-Dimensional Systems & Nanostructures 2007, 37, 44–48; d) F. Cesano, S. Bertarione, et al., Diam. Relat. Mater. 2009, 18, 979–983; e) J. Huo, H. Song, et al., Materials Chemistry and Physics 2007, 101, 221–227; f) X. Gong, Z. Guo, et al., Energy Fuels 2009, 23, 4547–4552; g) S. Bertarione, D. Scarano, et al., Chem. Mater. 2005, 17, 5119–5123; h) M. Inagaki, T. Masahiro, et al., RSC Advances 2015, 4, 41411–41424.

[21] a) D. Takagi, Y. Homma, et al., Nano Letters 2006, 6, 2642–2645; b) A. Primo, I. Esteve-Adell, et al., Angew. Chem. Int. Ed. 2016, 55, 607 -612.

[22] a) K. J.J. , R. B. Wilson, J. Appl. Chem. 1960, 10, 109–113; b) C. H. Giles, A. P. D'Silva, et al., in Proc. Int. Symp. Surface Area Determination (Ed.: D. H. E. a. R. H. Ottewill), Butterworths, Bristol, UK, 1969.

[23] S. Cravanzola, F. Cesano, G. Magnacca et al., RSC Advances 2016, 6, 59001–59008 K.

[24] a) S. Cravanzola, S. M. Jain, F. Cesano et al., RSC advances 2015, 5, 103255–103264; b) F. Cesano, G. Fenoglio, L. Carlos et al., Applied Surface Science 2015, 345, 175–181.

[25] a) K. Yuan, R. Che, et al., ACS Applied Materials & Interfaces 2015, 7, 5312–5319; b) K. Takai, T. Suzuki, et al., Carbon 2012, 73, 1436–1439; c) M. Bystrzejewski, Z. Karoly, et al., Carbon 2009, 47, 2040–2048; d) M. H. Al-Saleh, U. Sundararaj, Carbon 2009, 47, 2–22.

Magnetic hybrid carbon via graphitization of polystyrene-co-divinylbenzene: morphology, structure and adsorption properties.

Federico Cesano *[a], M. M. Rahman [a], F. Bardelli [a], A. Damin [a], and D. Scarano

[a] *Department of Chemistry, NIS (Nanostructured Interfaces and Surfaces) Interdepartmental Centre, University of Torino, Via P. Giuria, 7, 10125 Torino, Italy.*

Supporting Information.

a) Experimental Section.

Material preparation: Poly(4-ethylstyrene-co-divinylbenzene) (PS-*co*-DVB) and Iron(II) acetylacetonate ($Fe(ACAC)_2$) were purchased from Aldrich and used without any purification. Among polystyrene co-polymers, PS-co-DVB (polystyrene crosslinked with 80% of divinylbenzene, Sigma Aldrich, CAS#9043-77-0) has been selected because of its high pore accessibility (pores of 10-20 Å) and the cross-linked structure, which is important to avoid the melting upon thermal treatment. Fe(ACAC)2, as before mentioned, shows a good chemical affinity with polymers and organic matter. PS-co-DVB (4 g) was initially ground with liquid N_2 in a mortar. A first portion of the obtained fine powder (2g) was thermally treated into a quartz-tube furnace at 850°C for 0.5h, 2h and 5h under N_2 gas flow (Scheme 1, path 1 thermal pyrolysis), while the second portion of the ground sample was impregnated with a solution of $Fe(ACAC)_2$ in ethanol (100 mg/0.2L) and stirred for 48 h (Scheme 1, path 2). The solution was then filtered and the resulting powder was dried for 2 hours at 80°C, then placed into a quartz-tube furnace and thermally treated at the same temperatures for 0.5h, 2h and 5h under N_2 gas flow (100ml/min) (Scheme 1, path 2). The preparation of samples is schematized in Scheme 1.

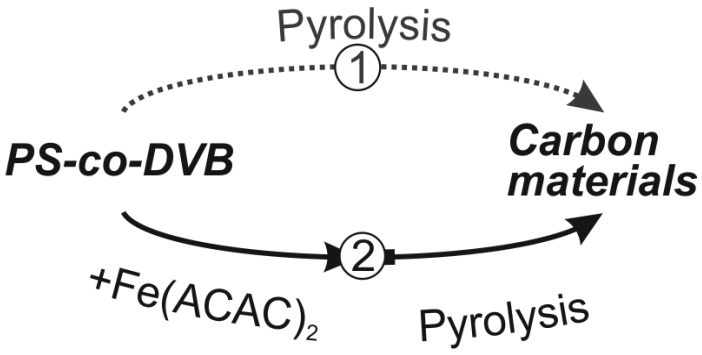

Scheme 1. Procedures for the sample preparation: (1) thermal treatment of the polymer under N2 and (2) thermal treatment after previous impregnation with $Fe(ACAC)_2$.

Material characterization: The pyrolysis process of the samples was followed by means of thermogravimetric analysis (TGA) (Q600-SDT TA instruments) by heating up to 850°C (heating rate 15°C/min) and the subsequent isothermal steps (a first isotherm under N_2 gas flow for 5h and a second one in air for 0.5 h) to be able to estimate both the carbon yield and the metal loading. Crystallographic phases, degree of crystallinity and the morphology were obtained on the pyrolyzed samples by means of X-ray diffraction (XRD) analysis, Raman spectroscopy, scanning electron microscopy (SEM) and transmission electron microscopy (TEM). XRD patterns were acquired using a PANalytical X'Pert PRO diffractometer equipped with a Cu source and a Ni filter, in a standard Bragg–Brentano geometry. The phase identification was obtained by comparing XRD patterns with the powder diffraction file (PDF) reference of the International Centre for Diffraction Data (ICDD). Vibrational properties of the samples were analyzed by μ-Raman measurements using a Renishaw inVia Raman microscope with a 785 nm wavelength laser and a 20xULWD objective; the total power on the sample was about 1 mWatt with a spot size of 1 μm in diameter. Up to fifty scans were acquired on different points of the samples and then averaged to increase statistics. The morphology and composition of samples were investigated by means of a Zeiss Evo 50 SEM instrument operating

at 30 kV, equipped with an energy dispersive X-ray (EDAX) detector. TEM images were obtained using a JEOL 3010-UHR instrument operating at 300 kV and equipped with a 2Kx2K pixel Gatan US1000 CCD camera. Samples were deposited on a copper grid covered by a lacey carbon film. Reciprocal lattices and simulated electron patterns to obtain crystal orientations were simulated by means of CaRIne Crystallography 3.1 software package. N_2 adsorption–desorption experiments have been carried out at 77 K (Micromeritics ASAP 2020 instrument) to determine the Brunauer–Emmett–Teller (BET) surface area and the micropore volume (t-plot method). Surface area measurements were performed after outgassing the samples at 400°C overnight. Pore size distributions (PSDs) were obtained by a non-negative least square curve fitting of the adsorption isotherm data by applying the Density Functional Theory (DFT) method (NLDFT model, carbon-slit-pores-method) with ASAP 2020 4.0 software (Micromeritics). Microporous (Smicro) and mesoporous (Smeso) surfaces were obtained from t-plot method (Carbon Black STSA thickness curve) and from Smeso= Stot – Smicro, respectively. Methylene Blue (MB) absorption experiments were obtained by means of the UV-vis spectroscopy (Varian Cary UV 5000) at RT.

100 ml of a 25 mg/l MB solution was prepared and contacted with 24 mg of the hybrid carbon material.

b) XRD Diffraction patterns of the polymer without and with the graphitization catalyst and treated at different temperatures

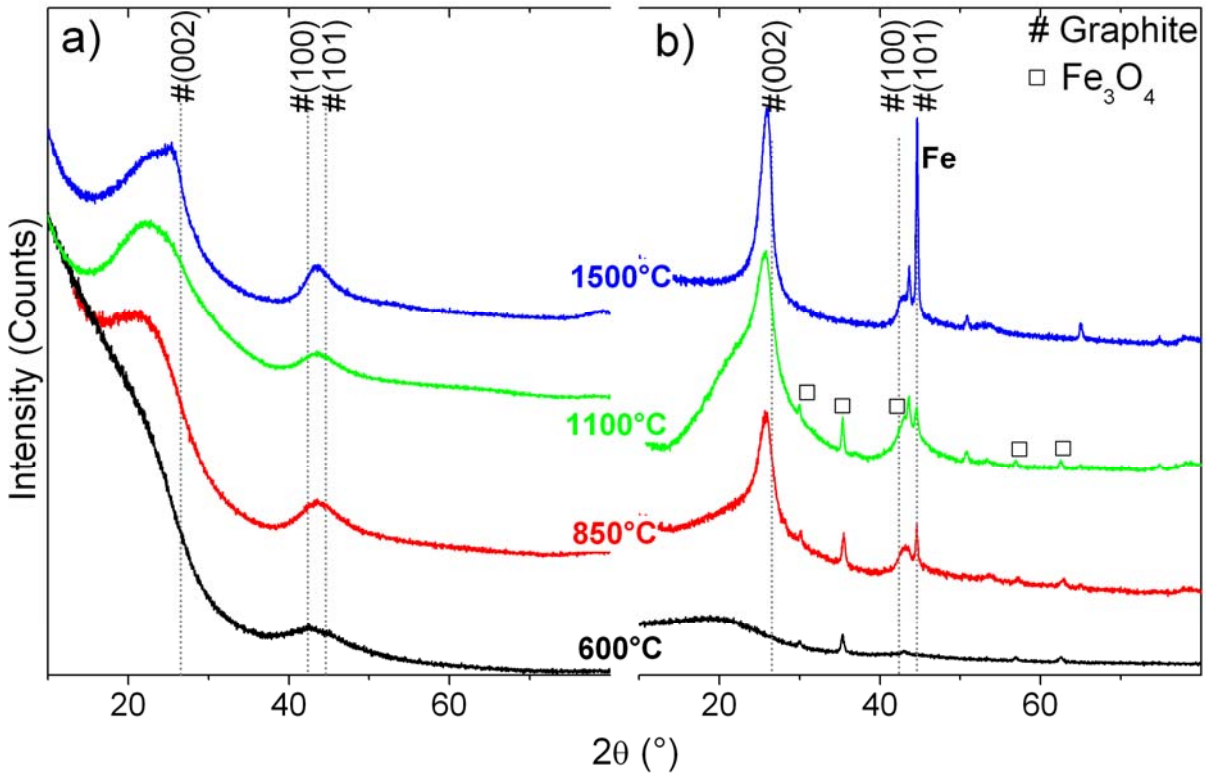

Figure S1. XRD patterns of a) the polymer and of b) Fe(II)/PS-co-DVB treated at 600°C, 850°C, 1100°C and at 1500°C, respectively.

c) N_2-Adsorption/desorption isotherms and pore-size distributions.

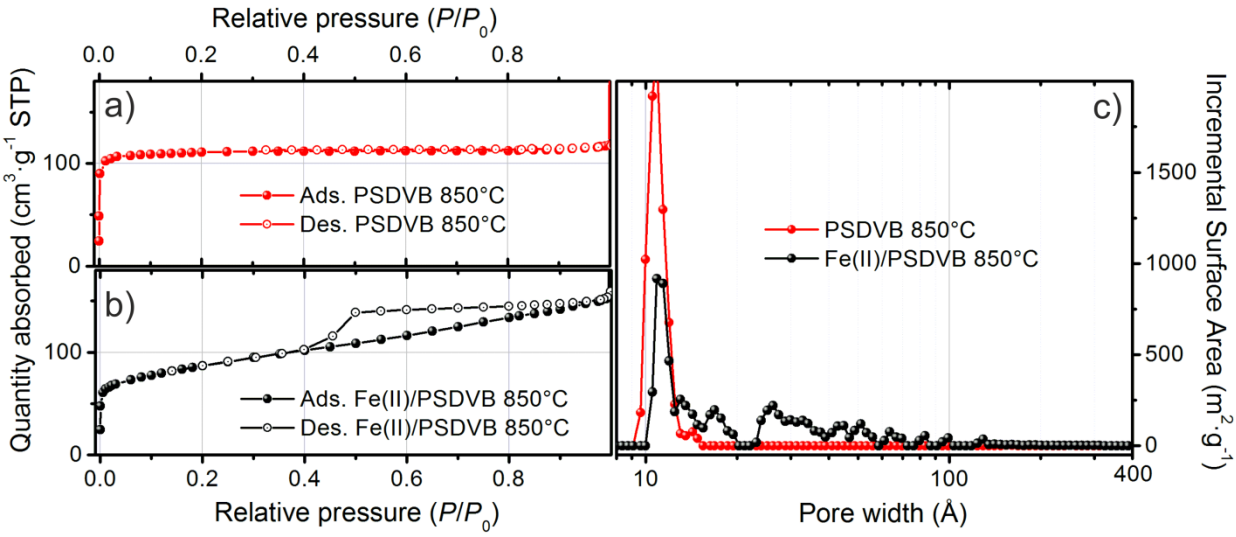

Figure S2. a) and b) N_2-adsorption/desorption isotherms and c) pore size distributions of PS-*co*-DVB and Fe(II)/PS-*co*-DVB samples treated at 850°C for 5h, respectively.

d) Methylene blue adsorption experiments.

Contact time effect. Concentrations of the residual dye solutions were measured at selected contact time (4, 12, 21, 29, 36, 42, 56, 66, 156 minutes) by monitoring the maximum absorbance values (λ_{max} = 661 nm) for the MB dye of the solutions by using the formula (*).

Langmuir plot. Adsorption isotherms were obtained from seven separated and weighed sample fractions for each carbon adsorbent in the 0.001g-0.100g range, placed in cylindrical flasks for 72 h to reach the equilibrium at RT, each containing 100 ml of 25 mg/l of the MB solution.
Absorbance intensities of solutions were determined at 661 nm by UV-vis spectroscopy (Varian Cary UV 5000) after 72 h on supernatant solutions. It was found that in the concentration range the MB solutions obeys the Beer-Lambert law.

The Langmuir adsorption isotherm, which assumes that a monolayer of material (MB) is adsorbed over a uniform adsorbent surface, may be written† as:

$$\frac{1}{x} = \frac{1}{x_m K} \cdot \frac{1}{c} + \frac{1}{x_m}$$

---

* Dye removal percentage $= \dfrac{(C_0 - C_t)}{C_0} \cdot 100$,

where C_0 and C_t are the initial concentration (25 mg/ml, 10 ml) and the concentration at the time t (mg/L), respectively.

† where x = adsorbed MB per mass of adsorbent, x_m = limiting amount of adsorbate per mass of adsorbent, K is constant, and c the concentration of the solute in equilibrium with the adsorbent.

1/x vs. *1/c* plot is expected to be linear with a gradient of l/x·K and intercept of $1/x_m$, on the 1/x axis:

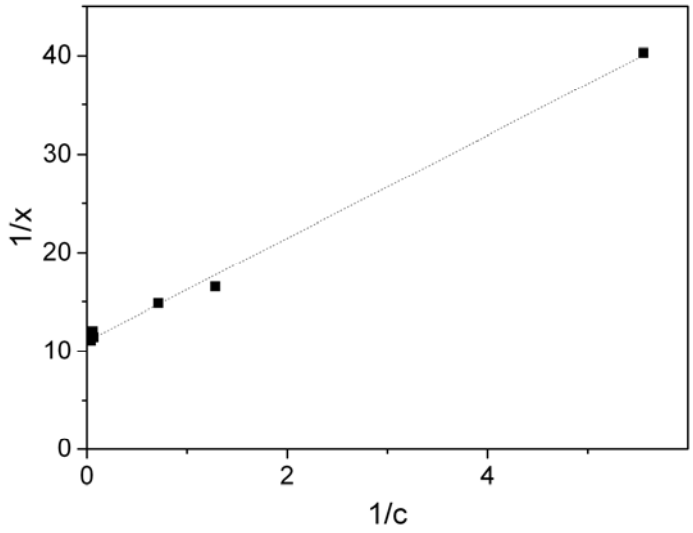

Figure S3. Langmuir linear-plot determined for the adsorption of 2.5 mg MB on selected weight portions of the hybrid graphitic material at 25°C.

e) Surface area determination of the hybrid carbon material from the MB adsorption experiments.

The approximate specific area (S) of the hybrid sample can be obtained from the dye adsorption isotherm. In more details, from the x_m value of the *1/x* vs. *1/C* plot (Figure S3) by considering the MB molecular weight and by applying the formula‡ $S = x_m \cdot N \cdot a$ (where *S* is specific surface area, *N* is the Avogadro's number and *a* is the area of the dye molecule, for MB *a*= 120 Å^2), a specific area value of ~205 m^2/g has been calculated for the hybrid sample obtained at 850°C.

f) Macroscopic magnetic properties of the hybrid porous graphitic powder.

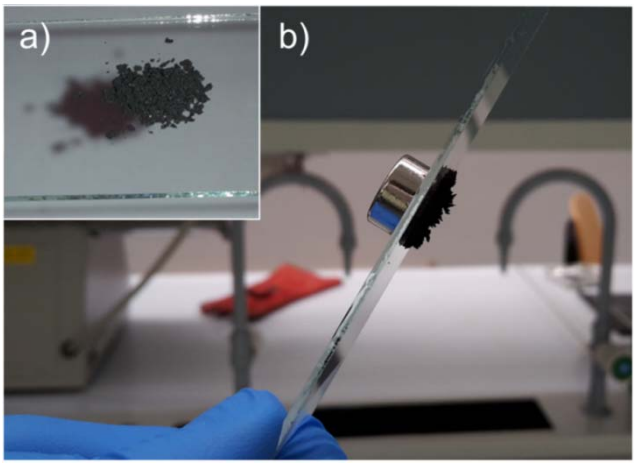

Figure S4. Pictures showing: a) the hybrid porous graphitic material, obtained at 850°C for 5h, which has been placed on a microscope glass slide and b) the same sample attracted by an approaching permanent magnet.

‡ Potgieter JH. *Adsorption of Methylene Blue on Activated Carbon. An Experiment Illustrating Both the Langmuir and Freundlich Isotherms*. J Chem Edu. 1991; 68:349-50.

g) UV-Vis spectra of the hybrid porous graphitic water suspension.

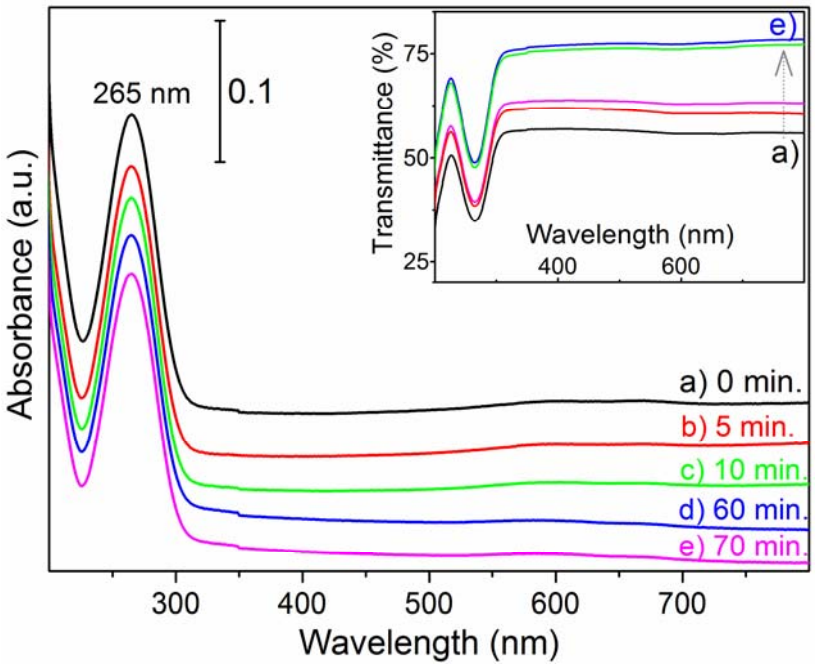

Figure S5. UV-Vis spectra of the hybrid porous graphitic suspension in water (0.5 mg/ml) after selecting the sonication time of ageing: a) as is, b) 5 min, c) 10 min, d) 60 min and e) 70 min. In the inset, spectra in transmittance are shown.